DEFORMATION MODES γ' PRECIPITATION HARDENED NICKEL-BASE ALLOYS

B. Kear, J. Oblak

JOURNAL DE PHYSIQUE *Colloque* C7, *supplément au n°* 12, *Tome* 35, *Décembre* 1974, *page* C7-35

DÉFORMATION MODES IN γ' PRECIPITATION HARDENED NICKEL-BASE ALLOYS

B. H. KEAR and J. M. OBLAK

Materials Engineering and Research Laboratory,
Pratt & Whitney Aircraft,
Middletown, Connecticut 06457, U. S. A.

Résumé. — Une étude détaillée des conséquences géométriques du cisaillement dans les précipités γ' de structure Ll_2 et des relations de compatibilité avec la matrice de structure cfc a permis de définir les modes de cisaillement possibles dans les alliages à base de nickel durcis par la précipitation de la phase γ'. La plupart de ces modes de déformation ont en fait été observés. Les mécanismes prédominants sont, à basse température, le glissement dans les plans { 111 } de paires $a/2 < 110 >$ et, à haute température, le cisaillement visqueux des précipités γ' par montée de paires $a/2 < 110 >$. Les modes de cisaillement par propagation de fautes d'empilement $a/3 < 112 >$ sont d'importance secondaire, sauf en fluage primaire à température intermédiaire où la propagation de paires de défauts intrinsèque et extrinsèque de surstructure contrôle la vitesse de déformation.

Abstract. — By a detailed consideration of the geometrical consequences of shear displacements in Ll_2 γ' and the requirement of compatibility with the fcc γ matrix, it has been possible to define the shear modes potentially operative in γ' precipitation hardened nickel-base alloys. Most of these geometrically possible deformation modes have, in fact, been observed. The predominant mechanisms are planar glide on { 111 } of paired $a/2 < 110 >$ dislocations at low temperature and viscous cutting of γ' by paired $a/2 < 110 >$ in climb configurations at high temperature. The $a/3 < 112 >$ stacking fault modes of shear are of secondary importance, except in primary creep at intermediate temperatures where the motion of superlattice intrinsic/extrinsic stacking fault pairs is rate controlling.

1. **Introduction.** — Nickel-base superalloys are essentially Ni-Cr solid solution alloys that have been strengthened by additions of Al and Ti to precipitate the γ'-phase, $Ni_3(Al, Ti)$. In addition, the alloys usually contain refractory metals (W, Mo, etc.) for solid solution strengthening and trace amounts of Zr, B and C to promote grain boundary strength.

During the past decade, much effort has been devoted to documenting the assorted microstructure/mechanical property relationships that are characteristic of γ' precipitation hardened nickel-base alloys [1-3]. As a result, fairly explicit models have been developed to account for the known yielding [4-8] and creep [9, 10] behavior of these materials. In this article, an attempt will be made to highlight the important developments from a strictly mechanistic viewpoint. Starting with simple geometrical considerations concerning the nature of planar faults in Ll_2, it will be shown that it is possible to deduce the various configurations for dissociated dislocations in γ' and, in turn, the various possibilities for dislocation/γ' particle interactions in the precipitation hardened alloys.

2. **Configurations for dissociated dislocations in the Ll_2 structure.** — 2.1 PLANAR FAULTS. — Three types of planar fault can be generated in Ll_2 by shear displacements on close-packed, ordered { 111 } planes. These are complex faults, antiphase boundaries, and superlattice intrinsic (or extrinsic) stacking faults, corresponding with shear displacements of the type $a/6 < 112 >$, $a/2 < 110 >$ and $a/3 < 112 >$, respectively, and represented by displacements 1, 2 and 3 in figure 1. Displacements 1 and 2 bring adjacent close-packed { 111 } planes into faulted positions where Al atoms have incorrect nearest neighbors. This is an unfavorable configuration, so that both complex fault (CF) and antiphase boundary (APB) tend to have high energies. On the other hand, shear displacement 3, which creates a superlattice intrinsic stacking fault (S-ISF) with correct nearest neighbor bonds, represents a configuration of low energy.

2.2 FUNDAMENTAL DISLOCATION DISSOCIATIONS. — It is convenient to describe dislocations in Ll_2 according to Thompson's notation [11], with Bδ, δA, etc. for

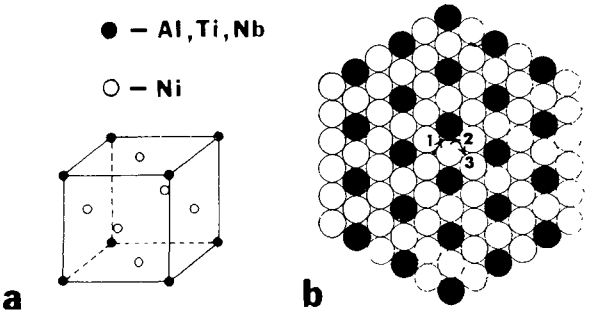

FIG. 1. — Arrangement of atoms in an A_3B compound with Ll_2 structure (*a*) unit cell, (*b*) close-packed octahedral plane.

$a/6 < 112 >$ Shockley partials, BA, CA, etc. for $a/2 < 110 >$ dislocations, and 2 Bδ, 2 δA, etc. for $a/3 < 112 >$ superlattice partial dislocations. Following Weertman [12], in order to distinguish between S-dislocations connected to single (intrinsic) stacking faults and D-dislocations connected to double (extrinsic) faults, a bar will be placed over the notation for a dislocation connected to a double stacking fault, e. g. 2 $\overline{\text{B}\delta}$, 2 $\overline{\delta\text{A}}$, etc. In addition, a system of symbols will be used to designate dislocation character, i. e. whether of edge, screw or mixed character. The system of symbols in Table I gives a unique meaning with

TABLE I

Correspondence between dislocation symbolism and dislocation character

⊥	edge
L	.. mixed edge and right-handed screw
⅃	.. mixed edge and left-handed screw
⌐	.... right-handed screw
¬	... left-handed screw

respect to dislocation character provided that the view is taken along the direction of the assigned dislocation tangent vector. For an intrinsic dissociation of a dislocation with net Burgers vector BA in the fcc structure, Thompson's rule states that the right-hand component is Bδ and the left-hand component is δA, provided that the dislocation is viewed from outside the reference tetrahedron in the direction of the tangent vector. It should be emphasized that in the Ll_2 structure the opposite rule applies for a superlattice dislocation with net Burgers vector 2 BA that dissociates into 2 Bδ and 2 δA. In Thompson's notation, the fundamental dissociations in Ll_2 [13-15] may be represented as follows :

$$2\,\text{BA} \rightarrow \underset{(\text{B}\delta + \delta\text{A})}{\text{BA}} + \underset{(\text{B}\delta + \delta\text{A})}{\text{BA}} \qquad \text{(i)}$$

$$2\,\text{BA} \rightarrow \underset{(\delta\text{C} + \text{B}\delta + \delta\text{A})}{2\,\text{B}\delta} + \underset{(\text{B}\delta + \delta\text{A} + \text{C}\delta)}{2\,\delta\text{A}} \qquad \text{(ii)}$$

Dissociation (i) gives a pair of dislocations that are coupled together by antiphase boundary (APB), with each dislocation further dissociated into a pair of Shockley partials coupled together by complex fault (CF) (Fig. 2*a*). The equilibrium width of such a

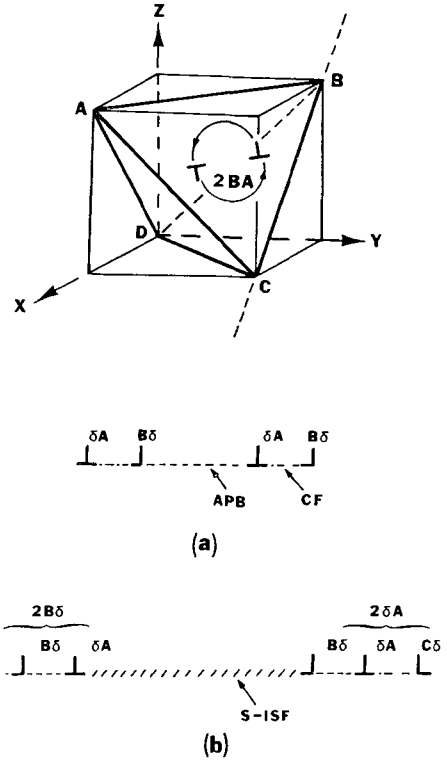

FIG. 2. — Reference tetrahedron ABCD and two possible dissociations for the dislocation loop 2 BA. Dislocation symbols correspond with direction CB in the reference tetrahedron.

superlattice dislocation is determined by the balance between the tensions exerted by the faults and the repulsive forces experienced by the constituent partial dislocations. The equilibrium width of the dislocation array is sensitive to APB energy — the higher the APB energy, the narrower the dislocation width, i. e. the more tightly constricted the entire dislocation array. In stoichiometric Ni_3Al (γ' phase) the equilibrium width for a dissociated dislocation of screw character is $\sim$ 30 Å ; the extent of the dissociation of the Shockley partials is only $\sim$ 5 Å. Dissociation (ii) gives a pair of superlattice partials that are coupled together by superlattice intrinsic stacking fault (S-ISF), with each partial comprising a triplet of Shockley partials (Fig. 2*b*). This configuration is much more

relaxed, i. e. widely extended, than the APB type, owing to the much lower energy of the S-ISF fault. Calculations indicate that the S-ISF dissociation becomes competitive with the APB type in materials with high APB energy. This is because the reduced interaction energy of the relaxed dislocation array more than offsets the higher core and elastic energies of the 2 Bδ-type dislocation compared with the BA type.

2.3 DISLOCATION INTERACTIONS. — Interactions between dislocations can also give rise to dissociated dislocations, which can take a variety of forms [16]. Some of the more interesting possibilities are as follows :

$$2\,\mathrm{BA\,(d)} + 2\,\mathrm{DB\,(a)} \rightarrow$$
$$\rightarrow \mathrm{BA\,(d)} + \mathrm{DA} + \mathrm{DB\,(a)} \quad (1)$$
$$\rightarrow 2\,\delta\mathrm{A} + 2\,\mathrm{D}\alpha + 2\,\alpha\delta \quad (1a)$$

$$2\,\mathrm{BA\,(d)} + 2\,\mathrm{CD\,(a)} \rightarrow$$
$$\rightarrow \mathrm{BA\,(d)} + \mathrm{BA/CD} + \mathrm{CD\,(a)} \quad (2)$$
$$\rightarrow 2\,\delta\mathrm{A} + 2\,\alpha\mathrm{D} + 2\,(\delta\alpha : \mathrm{AD}) \quad (2a)$$

$$2\,\mathrm{BA\,(d)} + 2\,\mathrm{DC\,(a)} \rightarrow$$
$$\rightarrow \mathrm{BA\,(d)} + \mathrm{BA/DC} + \mathrm{DC\,(a)} \quad (3)$$
$$\rightarrow 2\,\mathrm{B}\delta + 2\,\alpha\mathrm{C} + 4\,\alpha\delta \quad (3a)$$

$$2\,\mathrm{BA\,(d)} + 2\,\mathrm{BC\,(d)} \rightarrow$$
$$\rightarrow \mathrm{BA/BC\,(d)} + \mathrm{BA/BC\,(d)} \quad (4)$$
$$\rightarrow 2\,\mathrm{B}\delta + 2\,\mathrm{B}\delta + 2\,\overline{\mathrm{B}\delta} \quad (4a)$$

$$2\,\mathrm{BA\,(d)} + 2\,\mathrm{CB\,(d)} \rightarrow$$
$$\rightarrow \mathrm{CA\,(d)} + \mathrm{CA\,(d)} \quad (5)$$
$$\rightarrow 2\,\mathrm{C}\delta + 2\,\delta\mathrm{A} \quad (5a)$$

Reactions (1) and (1*a*) are two equivalent cases corresponding with the configuration of a Lomer-Cottrell lock in the fcc structure (Fig. 3). The product of reaction (1*a*) is favored in materials with high APB energy, since the reduced interaction energy of the relaxed array more than offsets the higher energies of the individual dislocations. Reaction (1) yields a truly sessile configuration in that the products of reaction (2 DA)

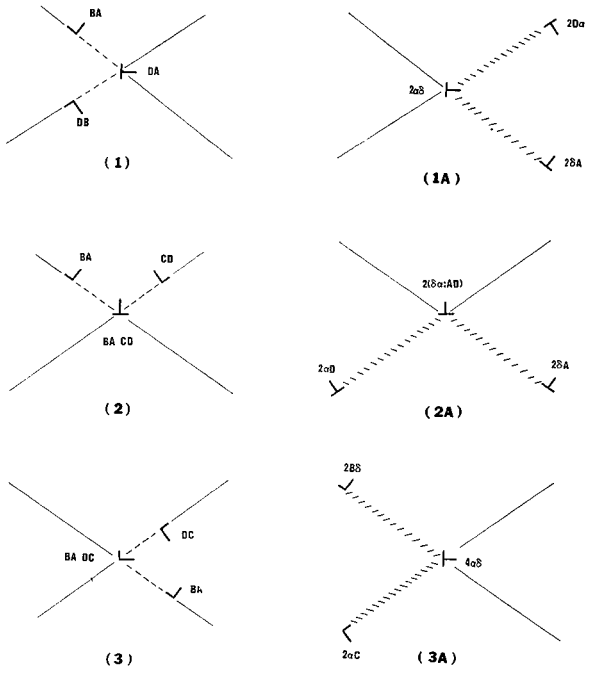

FIG. 3. — Possible configurations for products of dislocation interactions involving APB-coupled dislocation pairs. Dislocation symbols are appropriate for reaction line CB in figure 2.

can glide only in (010), which is not an easy slip plane in Ll_2 at low temperatures. Reaction (1*a*), however, is not completely sessile in that the reaction products 2 δA and 2 Dα are free to glide ; only the stair-rod 2 $\alpha\delta$ is immobile. This is illustrated in figure 4*a* for the more realistic case of a junction reaction occurring under an applied compressive stress parallel to AD. In this particular scheme, the operative shear stress driving the dislocations is actually higher for the segments 2Dα and 2 δA than for 2 DB and 2 BA dislocations, so that it is not unreasonable that they should glide with the dislocations even though they must leave behind ribbons of low energy stacking fault. For completeness, the trailing segments 2 αB and 2 Bδ are shown in relaxed cross slip configurations, see Section 2.4. Reactions (2), (2*a*), (3) and (3*a*) also yield

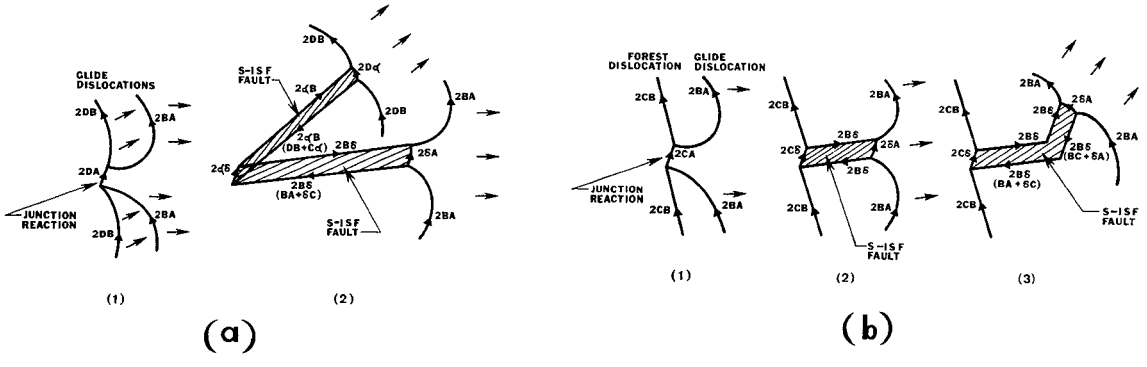

FIG. 4. — Illustrating formation of stacking fault ribbons by junction reactions involving APB-coupled dislocation pairs. Sense of dislocation motion is appropriate for a compressive stress parallel to AD in figure 2, with the junction reaction line parallel to CB.

symmetrical barrier configurations (Fig. 3), but again the products of reactions (2*a*) and (3*a*) are not completely sessile, as is the case for reactions (2) and (3). Junction reactions can also be envisaged where a high driving force acts on the potentially mobile dislocation segments, which would tend to drive these segments away from the junction, as in the preceding case. Reactions (4) and (4*a*) represent the case of co-planar double slip. The product of reaction (4), assuming that it goes to completion, consists of a pair of BA/BC ≡ 3 Bδ dislocations that are coupled together by a two-layer APB. In materials with high APB energy, this is obviously an unfavorable configuration. The alternative scheme represented by reaction (4*a*) has a much lower energy, since the dislocations are coupled together by low energy stacking faults. This particular arrangement, shown in detail in figure 5*a*,

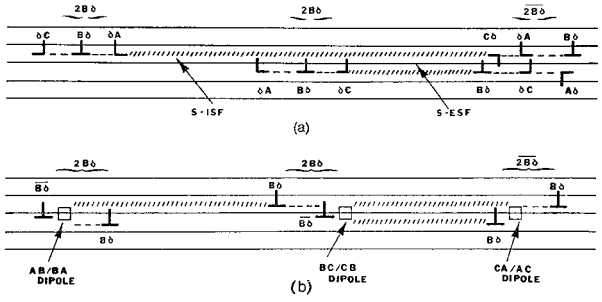

FIG. 5. — Two possible configurations for a superlattice intrinsic/extrincic fault pair with 6 B$\delta \equiv a <112>$ net Burgers vector. The symbol □ is used to indicate dipole displacements.

is known as a superlattice intrinsic/extrinsic stacking fault pair [16]. Reactions (5) and (5*a*) represent the alternative case of co-planar double slip, where all the reaction products are glissile. Reaction (5) need not go to completion, since a stable arrangement of dislocations in the sequence BA-CA-CB, i. e. a stable triple dislocation, can occur [17]. Under realistic circumstances, where a glide dislocation 2 BA interacts with, say, a stationary forest dislocation 2 CB, reaction (5*a*) may be preferred. This is illustrated in figure 4*b* for the case of a compressive stress parallel to AD. If the attractive junction is only a few Burgers vectors in length, it may be easier to bow out the segment 2 δA than the dislocation pair 2 CA. This mechanism is favored by a higher operative shear stress on 2 δA than on 2 CA. Also shown in figure 4*b* are the two preferred directions for 2 Bδ dislocations that form the boundaries of the ribbon of stacking fault dragged out by the glissile 2 δA dislocation segment, see Section 2.4. A similar junction reaction involving glide and forest dislocations could also generate an intrinsic/extrinsic stacking fault pair.

2.4 DISLOCATION MOBILITY AND FLOW STRESS OF γ'. — Since the APB energy in Ll_2 depends strongly on crystallographic orientation, the minimum energy configuration for a dislocation pair is usually not in the preferred {111} slip plane [18]. For example, an APB-coupled dislocation pair of screw character can reduce its energy by cross slip from (111) into (010), since the latter is a plane of low APB energy (Fig. 6*a*).

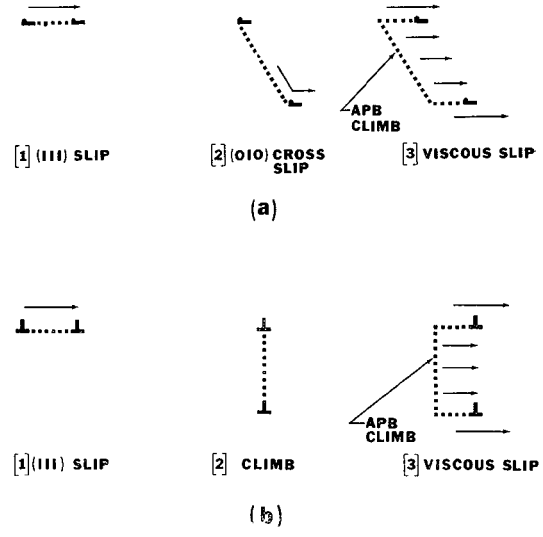

FIG. 6. — Schematic contrasting slip and viscous slip motions of APB-coupled dislocation pairs ; (*a*) screw dislocation pair, (*b*) edge dislocation pair. Note that viscous slip involves climb of APB's, irrespective of dislocation character.

Similarly, dislocation pairs of edge or mixed character can take up lower energy configurations by climb (Fig. 6*b*). Such effects can exert an influence on deformation behavior because they influence dislocation mobility. Thus, cross slip of a screw dislocation pair can be an effective dislocation pinning mechanism [19]. Again, if an edge (or mixed) dislocation pair assumes a climb-type configuration, its glide motion will thereafter be controlled by the climb rate of the coupling APB [18] (Fig. 6*b*). Another example of dislocation pinning that is a consequence of cross slip is shown in figure 7. In this case, a 2 δB dislocation becomes effectively pinned when its CB component undergoes cross slip into (010), leaving behind an Aδ Shockley partial at the boundary between the (010) APB and the (111) S-ISF fault [20]. A similar configuration is obtained if the AB component of the 2 δB dislocation cross slips into (001). In other words, for a 2 Bδ-type dislocation, this relaxation mechanism can occur in two directions in the original (111) slip plane, i. e. parallel to CB and AB in the reference tetrahedron ABCD (Fig. 2), but not parallel to AC.

Plastically deformed γ' exhibits a fine homogeneous slip line structure, and the slip dislocations are predominantly of screw character [21] (Fig. 8*a*). This has been interpreted to mean that screw dislocations are less mobile than edge dislocations because of a strong tendency for dislocation pinning by the cross slip mechanism shown in figure 6*a*. Under conditions of multiple slip, screw dislocations become interspersed

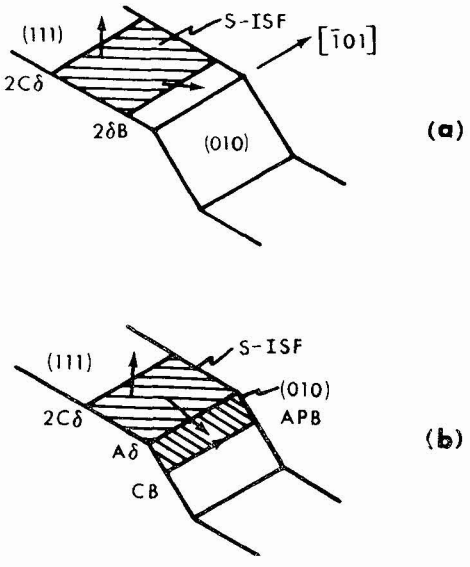

FIG. 7. — Pinning of a 2 δB superlattice partial dislocation as a result of cross slip of its CB component into (010).

with dislocation debris, usually in the form thin ribbons of stacking fault [20-23] (Fig. 8*b*, *d*) which appear to have their origin in dislocation interactions of the type shown in figure 4. Other than a reduction in the density of stacking faults, no significant differences in the general appearance of the deformed structure is observed with increasing temperature [21]. However, recent observations using the weak-beam technique for resolving the dislocation pairs have confirmed that the screw dislocation pairs lie in cube planes (Fig. 9) and that the measured separation of the pairs decreases monotonically with temperature [24]. This latter result is indicative of a strong inverse temperature dependence for the cube plane friction stress, suggesting that cross slip from {111} onto {100} becomes easier and double cross slip back into {111} more difficult with increasing temperatures, at least up to 760 °C. On this basis it is easy to explain the observed temperature dependence of the yield strength, and the distinction that must be made between the microyield strength and the 0.2 % offset yield strength ; only the latter is strongly temperature dependent [25] (Fig. 10). At low temperatures, it is envisaged that the dislocation loops expand freely in the edge and screw orientations, so that the average slip distance is large. Thus, there is not much difference between the measured microyield strength and the 0.2 % offset yield strength of the material. On the other hand, in the critical intermediate temperature range of interest, only the edge segments of the dislocation loops expand freely ; the screw segments experience a stick/slip-type of motion, as they undergo cross slip onto {100} and occasionally double cross slip back onto {111}. Under these conditions, the average slip distance should decrease with increasing temperature due to an increasing probability for effective trapping

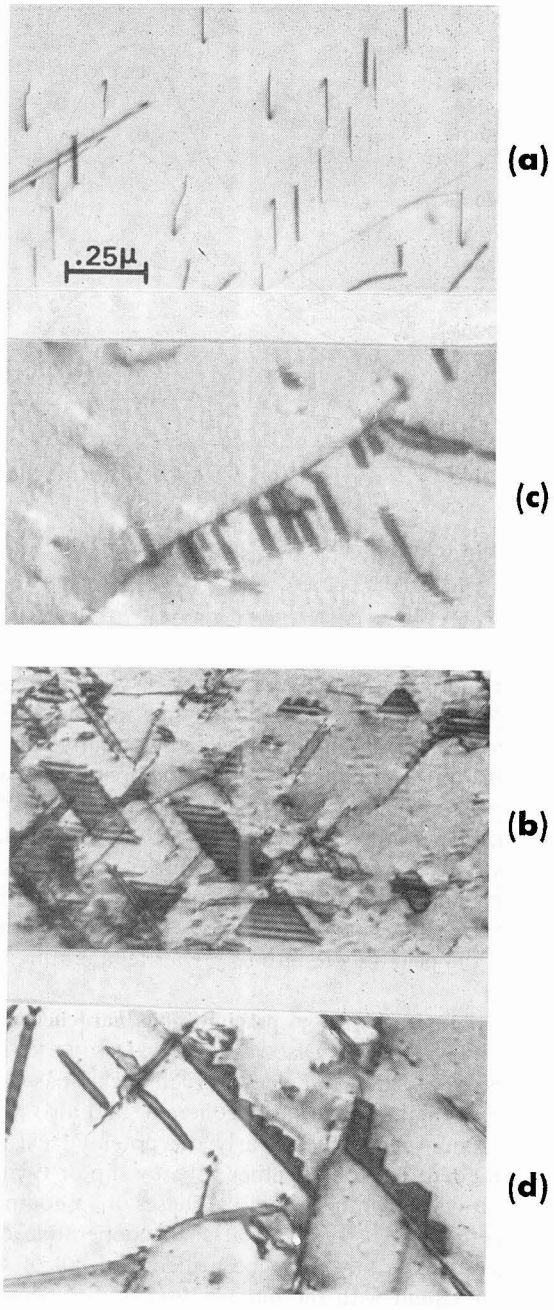

FIG. 8. — Deformation structures in γ' ; (*a*) arrangement of screw dislocations, (*b*) ribbons of stacking fault, and (*c*) stacking faults with sawtooth-shaped edges.

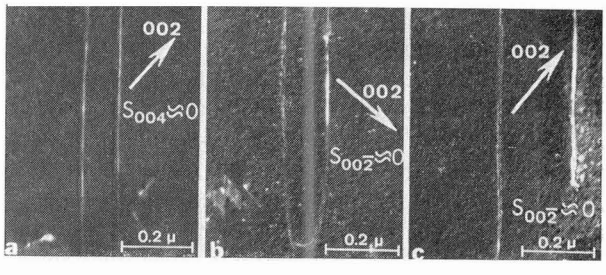

FIG. 9. — Cross slip into {100} at (*a*) 425 °C, (*b*) 320 °C and (*c*) 200 °C.

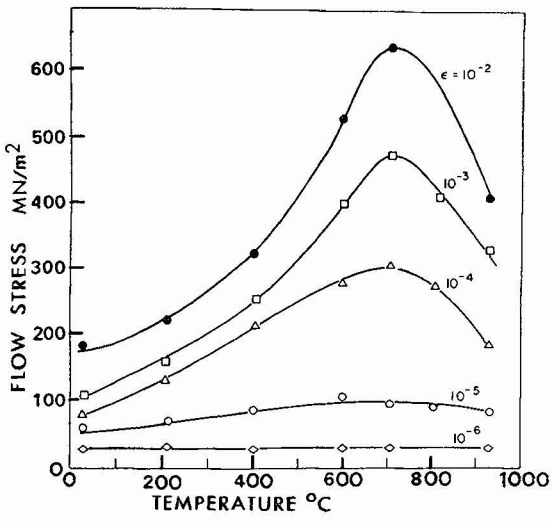

FIG. 10. — Yield stress versus temperature curves for Ni_3Al, γ' phase.

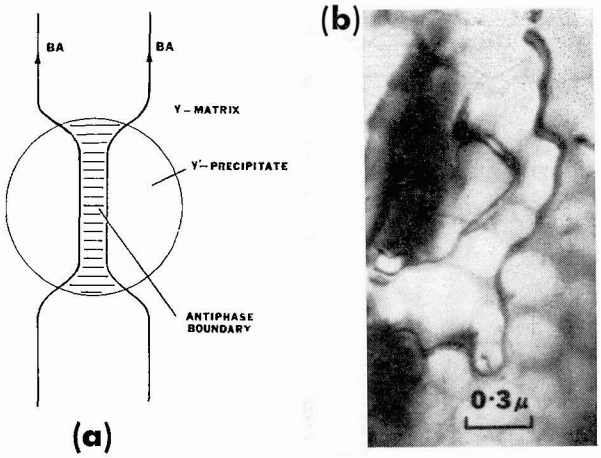

FIG. 11. — Slip plane section showing γ' particle shearing by APB-coupled dislocation pairs ; (*a*) schematic illustration of the constriction of pairs within γ', (*b*) pairs in alloy Mar-M200, showing relaxation in the γ matrix.

of screw segments of expanding dislocation loops. Such a decrease in average slip distance raises the 0.2 % offset yield strength, but has no effect on the microyield strength because the mobility of edge dislocations is unaffected. At high temperatures, where the yield strength falls off sharply, evidence has been obtained for diffusive slip of the type shown in figure 6. As would be expected, under these conditions, the macroyield strength is sensitive to strain rate ; increasing the strain rate raises the yield strength and shifts the peak in strength to higher temperatures [26].

3. **Deformation of γ' precipitations hardened nickel-base alloys.** — 3.1 DISLOCATION/γ' PARTICLE INTERACTIONS. — Since γ and γ' phases in nickel-base alloys are, in general, remarkably coherent, and also possess a common slip plane, clearly the potential exists for plastic deformation, whether it be by slip or twinning, that involves both γ and γ' phases in a completely cooperative manner. Several such cooperative deformation modes have now been identified, all of which are consistent with the models discussed in Section 2.

The most common slip mode in γ' precipitation hardened nickel-base alloys is shearing of the γ' particles by APB-coupled dislocation pairs [4, 27] (Fig. 11). During passage through the γ' particles, the dislocation pairs are tightly constricted, owing to the high energy of the coupling APB's. Slip, therefore, involves the alternate constriction and dissociation of dislocation pairs as they cut through γ' and γ, respectively. The dislocation pairs normally glide in groups, or avalanches, giving rise to intense dislocation slip traces and coarse surface slip offsets. In tensile tests, this APB-type slip mode prevails over a wide range of temperature — certainly up to ~ 850 °C at ordinary strain rates. At high temperatures, such that interactions between dislocation pairs and thermal vacancies become important, the pairs tend to assume new orientations of minimum total energy. Under these conditions, diffusive slip of the type illustrated in figure 6 becomes the rate controlling deformation mechanism [10] (Fig. 12).

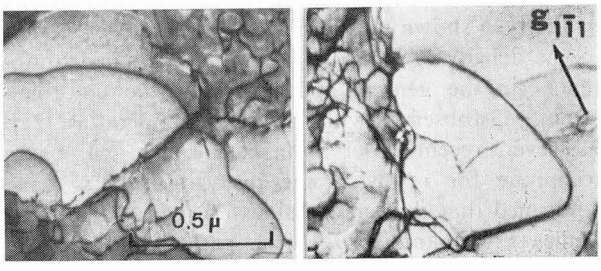

FIG. 12. — Shear of γ' by APB-coupled dislocation pairs during creep at high temperatures ; (*a*) dislocations in pairs not resolved individually at 855 °C, (*b*) pairs which have assumed climb configurations are resolved at 927 °C.

A low stacking fault energy γ matrix phase is characteristic of many nickel-base alloys, because alloying elements that partition preferentially to the γ phase, such as Co, Mo and, particularly, Cr reduce the stacking fault energy of Ni [28-30]. An important consequence of this is that certain dissociated dislocations in the γ matrix that repel one another at long-range can, in fact, experience a short-range attraction. This is because the constituent partial dislocations can arrange themselves as a so-called intrinsic/extrinsic fault pair [31, 32] with net Burgers vector 3 Bδ. Since the superlattice analogue to this reaction (reaction 4*a*) gives a product with net Burgers vector 6 Bδ, it follows that a pair of 3 Bδ γ matrix dislocations constitutes a perfect translation vector for shearing γ' particles. On the other hand, a single 3 Bδ γ matrix dislocation cutting through the γ' particles must necessarily generate stacking fault in the γ' phase. The two cases are represented schematically in figure 13.

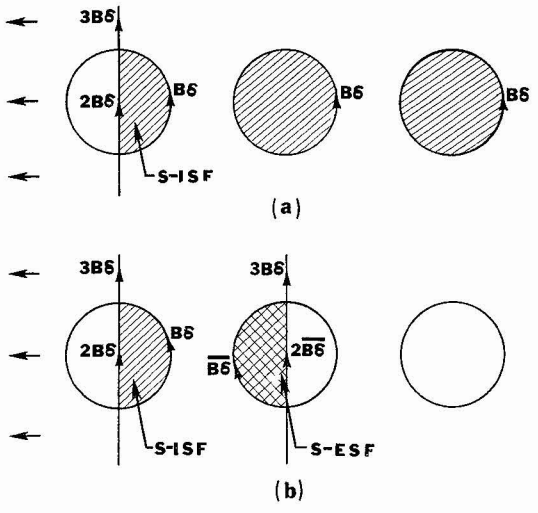

FIG. 13. — Shear of γ' particles by intrinsic/extrinsic fault pairs ; (*a*) formation of stacking faults in γ' by shear of a single 3 B$\delta \equiv a/2 < 112 >$ matrix dislocation, (*b*) coupled shear of γ' by a pair of 3 Bδ matrix dislocations.

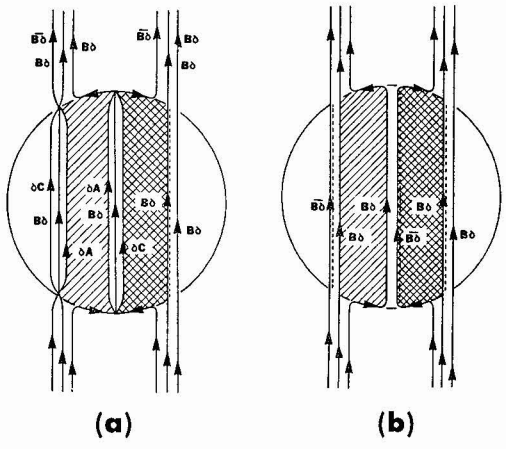

FIG. 14. — Details of dislocation dissociation in a γ' particle sheared according to the scheme illustrated in figure 13*b*. Cases (*a*) and (*b*) correspond with figures 5*a* and *b*, respectively

Close examination of the sequences of partial dislocations appropriate for such 3 Bδ-type matrix dislocations and 2 Bδ-type precipitate dislocations reveals that the partials comprising the 3 Bδ dislocations must undergo some kind of rearrangement at the γ/γ' interfaces, i. e. at the point of entry into the γ' particles [33]. In one scheme (Fig. 14*a*) the rearrangement involves dislocation constriction and crossover in order to generate the required sequence of partial dislocations in the γ' precipitate. In an alternative scheme (Fig. 14*b*), dislocation crossover is avoided by introducing

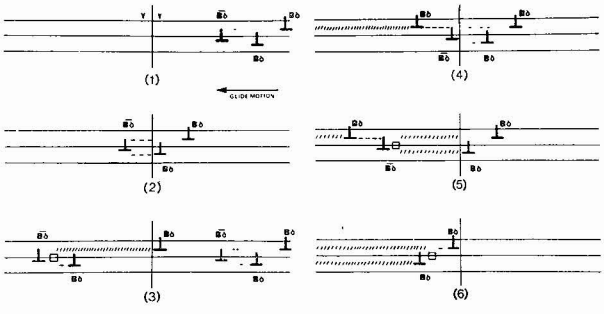

FIG. 15. — Details of the interaction between a pair of matrix 3 B$\delta \equiv a/2 < 112 >$ dislocations and a γ' particle.

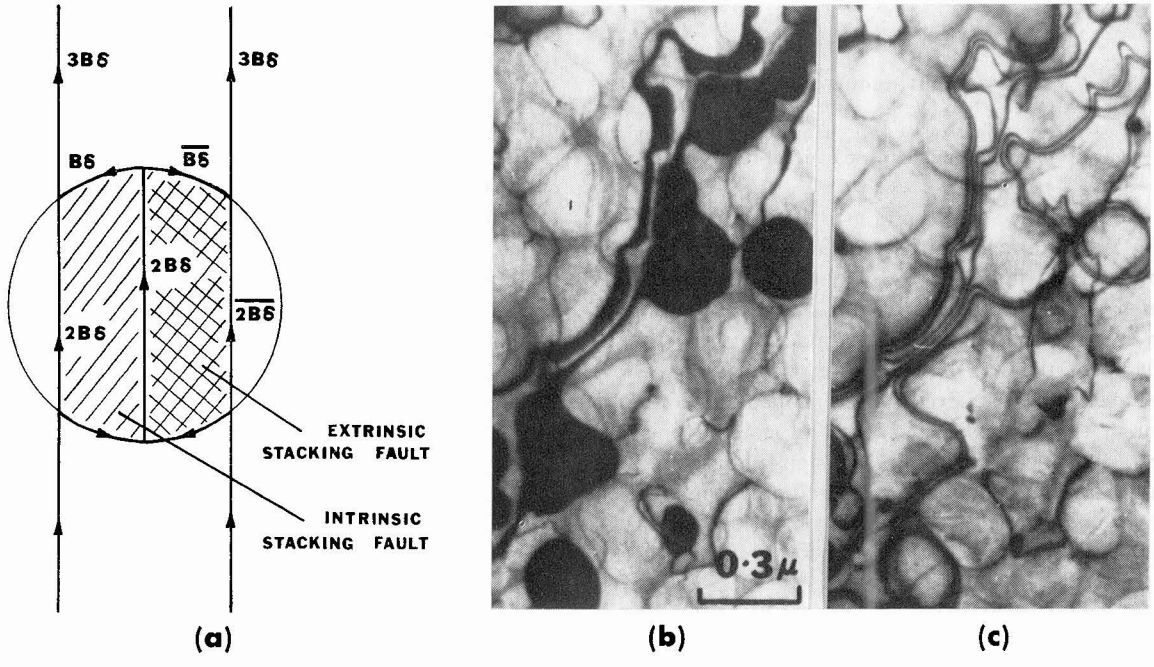

FIG. 16. — Slip plane section showing γ' particle shearing by 3 B$\delta \equiv a/2 < 112 >$ matrix dislocation pairs ; (*a*) schematic illustration of the shearing process involving a triplet of 2 B$\delta \equiv a/3 < 112 >$ superlattice partials, (*b*) intrinsic (S-ISF) and extrinsic (S-ESF) fault pair in alloy Mar-M200, (*c*) sequence of partial dislocations in the fault pair.

AB/BA-type dipole displacements (see Fig. 5*b*) at the positions indicated by dotted lines. Assuming such dipole displacements, figure 15 shows the orderly manner in which γ' precipitate can be sheared by the sequence of partial dislocations comprising the 3 Bδ matrix dislocations. Experimentally, it has been found that intrinsic/extrinsic shear is a common slip mode in nickel-base alloys deformed at intermediate temperatures [34-36]. In one case (Fig. 16), direct evidence was obtained for γ' particle shearing by the mechanism depicted in figure 14*b*, where individual Bδ-type partial dislocations extend from γ matrix into γ' precipitate without any visible constrictions or crossover.

For the case of γ' particle shearing by individual 3Bδ-type matrix dislocations, it is clear that the accumulation of stacking faults in the γ' phase can lead to twinning [35, 37]. The mechanism is illustrated in figure 17. Successive shears of the γ' particles by

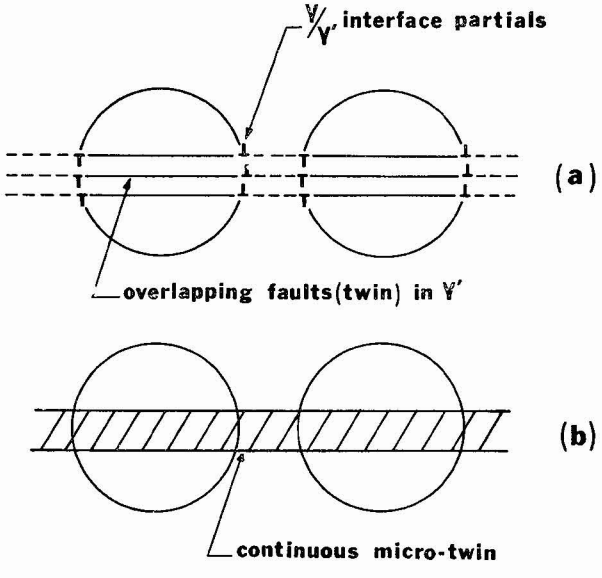

FIG. 17. — Illustrating proposed mechanism of micro-twinning in a γ' precipitation hardened nickel-base alloy.

3 Bδ dislocations creates a situation where energy minimization favors the formation of new faults alongside existing ones, resulting in the nucleation of thin twins in the γ' phase. At some point, the stresses built up by the arrays of Shockley partials at the γ/γ' interfaces will be relieved by the propagation of twins through the γ phase, as groups of neighboring γ/γ' interface dislocations of opposite signs undergo mutual annihilation. The final result, therefore, is the creation of twin lamellae, albeit somewhat imperfect in character, that extend through both γ and γ' phases (Fig. 18).

3.2 YIELD STRENGTH. — The yield strength of most nickel-base alloys is relatively insensitive to strain rate and temperature up to $\sim$ 760 °C. At higher temperatures, the strength is markedly strain rate dependent, and typically a small yield strength maxi-

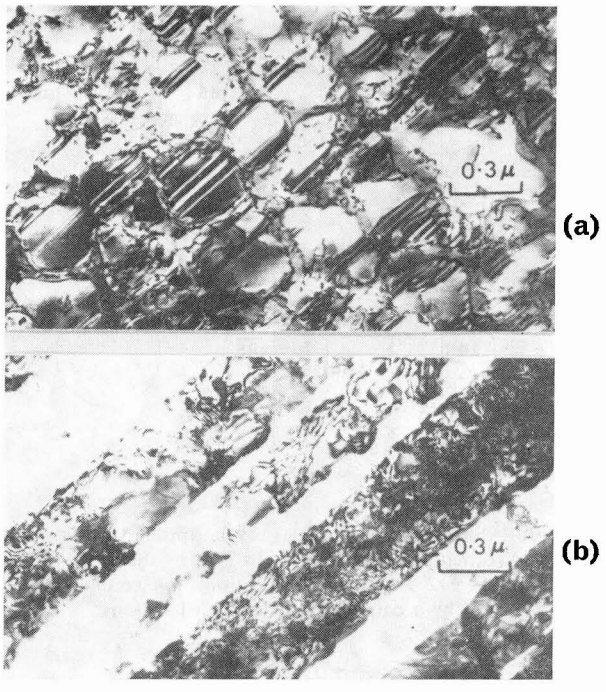

FIG. 18. — Microstructures developed after relatively large strains in creep of < 110 > oriented Mar-M200 ; (*a*) overlapping stacking faults in γ' phase, (*b*) microtwins extending through both γ and γ' phases.

mum occurs prior to a sharp decrease in strength [6, 26] (Fig. 19). These effects can be understood quite simply in terms of the known changes in the nature of dislocation/γ' particle interactions with increasing temperature. At temperatures below $\sim$ 760 °C, the γ' particles are sheared by dislocation pairs that are coupled together by APB (Fig. 11). In most alloys, the equilibrium width of the dislocation pair in the γ' particle is small, owing to high energy of the coupling APB. Under these conditions, the yield strength is determined primarily by the stress required to constrict the dislocation pair to the equilibrium width at the point of entry into the γ' particle. This APB-type strengthening makes a fixed and relatively large contribution

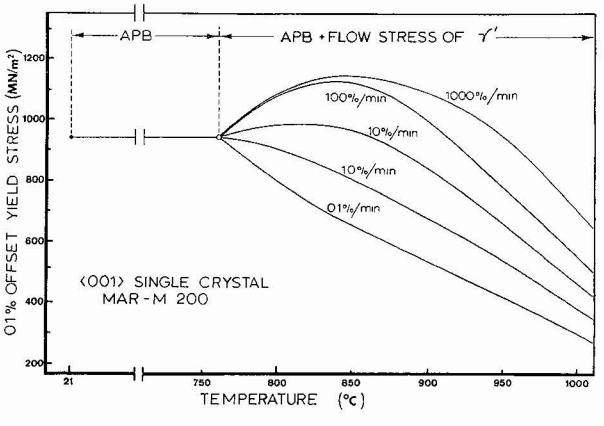

FIG. 19. — Temperature and strain rate dependence of the yield stress for < 001 > oriented Mar-M200.

to the yield strength at temperatures where diffusion plays no significant role in the deformation process [6]. At a strain rate $\sim$ 0.1 %/min, the maximum temperature for diffusionless APB-type shear is probably 855 °C. Under high strain rates, the maximum is pushed to higher temperatures. Whatever the strain rate, however, at some critical temperature diffusive slip of APB coupled dislocation pairs becomes the rate controlling deformation mechanism (Fig. 12), in which case the yield strength falls off with further increase in temperature (Fig. 19). Another complication arises because of the anomalous increase in the intrinsic strength of the γ' phase with increasing temperature (Fig. 10). Since this appears to be due to dislocation pinning as a result of thermally activated cross slip, and does not involve climb, it is to be expected that the strength of the γ' phase should influence the yield strength of the γ' particle strengthened alloy at temperatures below that where diffusive slip can take place easily. It is believed that this explains the peak in the strength of Mar-M200 at intermediate temperatures, and its shift to higher temperatures with increasing strain rate (Fig. 19).

3.3 CREEP BEHAVIOR. — Two distinct types of creep behavior [9, 10] have been identified in Mar-M200 ; intermediate temperature creep at 760 °C and high temperature creep at 855 °C. At 760 °C the creep curve exhibits an incubation period followed by an extended region of primary creep, whereas at 855 °C there is no incubation period prior to primary creep, and the primary creep strain is markedly reduced (Fig. 20). As will now be shown, this striking difference in creep behavior at these two temperatures clearly reflects fundamental differences in creep deformation mechanism, as would be expected.

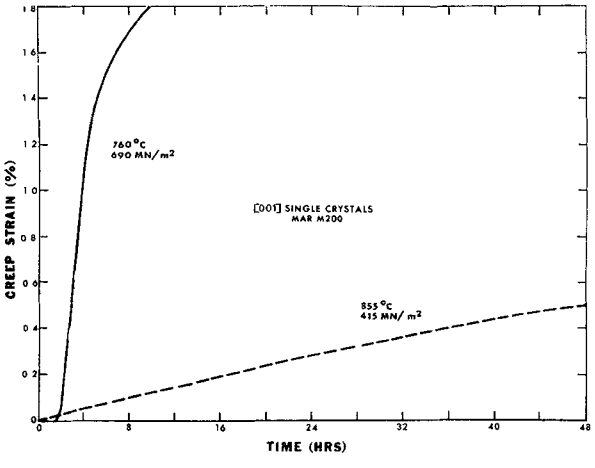

FIG. 20. — Comparison of short-time creep at 760 °C and 855 °C for < 001 > crystals of Mar-M200. Note the incubation period and extensive primary creep at 760 °C.

As shown in figure 21, the observed extent of primary creep at 760 °C is remarkably sensitive to crystallographic orientation. In orientation A, the primary creep strain is 1.7 %, whereas in orientation F, primary creep continues up to the point of fracture ; a total of 37 % creep strain. This orientation effect is a consequence of the fact that primary creep occurs by viscous slip of intrinsic/extrinsic fault pairs, i. e. by $\{111\} < 112 >$ slip, as described in Section 2.3. A larger slip distance is expected for such slip, owing to the widely extended nature of the dislocation array, which tends to prevent dislocations from leaving their slip planes by cross slip or climb. Since orientation F is an ideal orientation for $\{111\} < 112 >$ single slip, the large amount of primary creep may be ascribed to the unperturbed nature of the single slip. Intensive deformation in one slip system in this orientation has been confirmed by lattice rotation studies and by TEM. Moreover, the latter observations have shown that at relatively high strains, slip degenerates into twinning (Fig. 18) such that very thin lamallae are developed on the predicted primary system. In orientation A, four $\{111\} < 112 >$ systems are active in primary creep, and the extent of primary creep appears to be limited by the strain hardening due to interactions between dislocations gliding in intersecting systems. Evidence for this is presented in figure 22. It can be seen that the onset of steady state creep at approximately 1.35 % strain corresponds with the first appearance of a homogeneous dislocation network, i. e. a uniformly strain hardened state for the material. The extent of primary creep observed in other orientations is consistent with this model. Thus, unperturbed single slip should occur in orientations B and C, at least initially, which would explain the more extended period of primary creep than that found in orientation A. Steady state creep in these orientations sets in presumably when the lattice rotation (see arrows in the inset of Fig. 21) is sufficient to induce appreciable slip in other systems accompanied by strain hardening. Orientation C experiences more primary creep than orientation B since its initial orientation is furthest removed from the < 001 > multiple slip orientation.

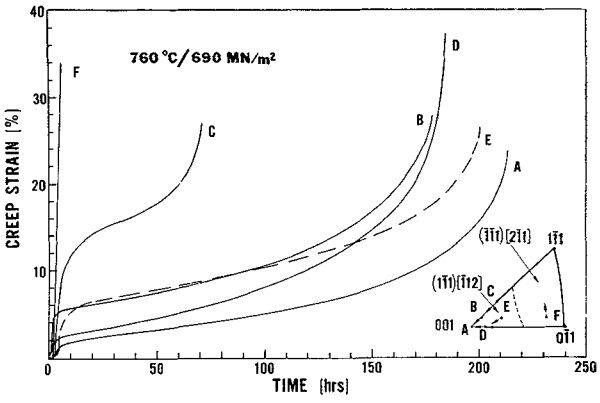

FIG. 21. — Creep curves for crystals of Mar-M 200 in various orientations at 760 °C.

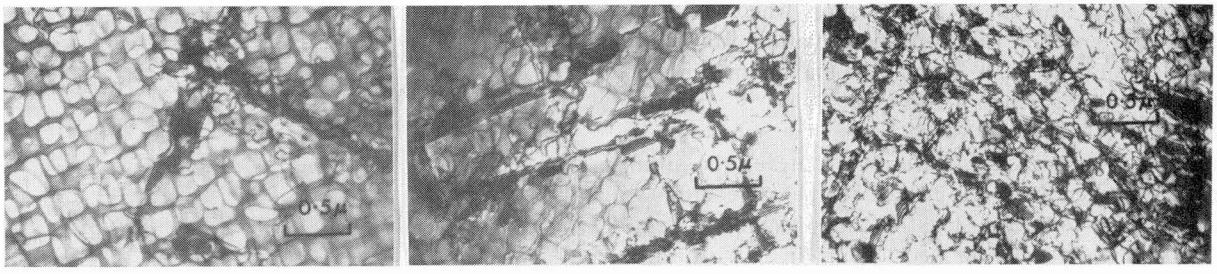

FIG. 22. — Development of strain hardening (intersecting slip) during primary creep at 760 °C for crystals with an < 001 > orientation ; (*a*) 0.35 pct. strain, (*b*) 0.80 pct. strain and (*c*) 1.35 pct. strain.

Following this same line of reasoning, the primary creep strain in orientation D is intermediate between that found in orientations A and B, because this happens to be an orientation favoring intersecting slip in two systems. In all orientations, the presence of an incubation period prior to the onset of primary creep (Fig. 20) probably reflects the lack of suitable sources for intrinsic/extrinsic shear in the original material. Thus, time is required to nucleate a sufficient density of the required $a/2 < 112 >$ dislocation sources, which will occur quite naturally as a result of interactions between $a/2 < 110 >$ dislocations in the γ matrix. It should be noted that the same considerations need not hold for polycrystalline material where grain boundaries appear to be direct sources for $a/2 < 112 >$ dislocations (Fig. 23).

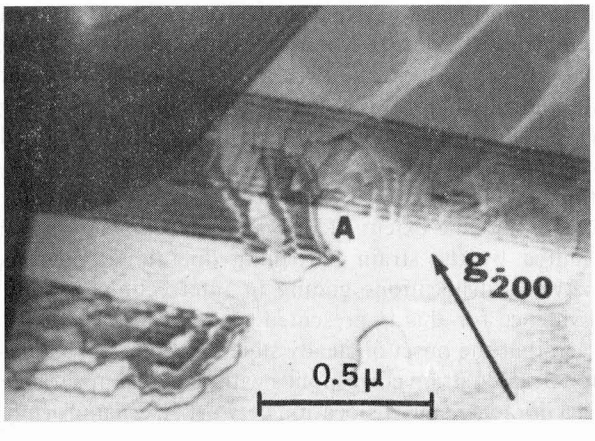

FIG. 23. — Grain boundary source for twinning in polycrystalline IN 100 deformed at 760 °C.

The extent of primary creep at 855 °C is not only much less than that at 760 °C (Fig. 20), but also is much less dependent on orientation (Fig. 24). The reason for this is that primary creep at 855° C occurs mainly by viscous slip of APB-coupled dislocation pairs (Fig. 12). Since this type of deformation is more homogeneous in nature than intrinsic/extrinsic shear, it takes less primary creep strain to establish the uniform distribution of dislocations characteristic of the steady state creep microstructure. The absence of an incubation period at this temperature may be attributed to the ability of the APB-coupled dislocation pairs to cut through the γ' particles at reasonable rates, albeit with the assistance of diffusion, from the outset of creep.

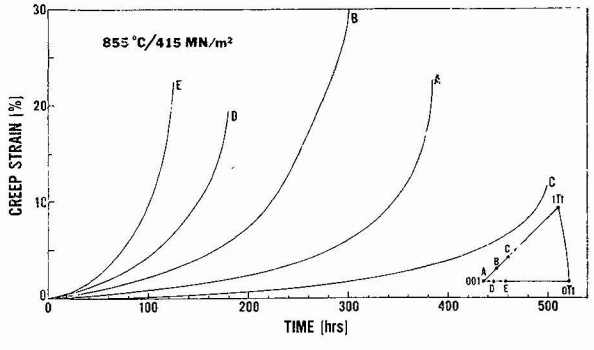

FIG. 24. — Creep curves for crystals in various orientations at 855 °C. Primary creep is all but absent, while the steady state creep rate is strongly dependent upon orientation.

In steady state creep, the rate controlling creep mechanism at 855 °C, and probably at 760 °C, is γ' particle shearing by diffusive slip of APB-coupled dislocation pairs (Fig. 12). Moreover, the creep microstructure consists of a characteristically uniform distribution of $a/2 < 110 >$ dislocations arranged for the most part in networks at the γ/γ' interfaces. Under these conditions, the average slip distance is probably of the order of the γ' particle size. Thus, it is envisaged that in steady state creep the networks act as both sources and sinks for dislocations, and that the creep rate is controlled by the density of mobile dislocations passing from one network to the next adjacent one through the γ' particles. The difference in steady state creep rates for the different orientations shown in figure 24 is related to the stability of the dislocation networks formed at the γ/γ' interfaces, which varies depending upon the activated slip systems. At higher temperatures, even this orientation effect is diminished [38].

References

[1] DECKER, R. F., Symposium on Steel Strengthening Mechanisms, Zurich, Switzerland, May 5-6, 1969.

[2] VERSNYDER, F. L. and SHANK, M. E., *Mat. Sci. & Eng.* **6** (1970) 213.

[3] *The Superalloys*, eds. C. T. Sims and W. C. Hagel (John Wiley and Sons, New York) 1972.

[4] GLEITER, H. and HORNBOGEN, E., *Phys. Stat. Sol.* **12** (1965) 235, 251.

[5] GEROLD, V. and HABERKORN, H., *Phys. Stat. Sol.* **16** (1966) 675.

[6] COPLEY, S. M. and KEAR, B. H., *Trans. Met. Soc. AIME* **239** (1967) 984.

[7] HAM, R. K., « *Ordered Alloys : Structural Applications and Physical Metallurgy* » (Claitors) Baton Rouge, Louisiana (1970) 365.

[8] BROWN, L. M. and HAM, R. K., « *Strengthening Methods in Crystals* » (Elsevier Amsterdam) 1971 9.

[9] LEVERANT, G. R. and KEAR, B. H., *Met. Trans.* **1** (1970) 491.

[10] LEVERANT, G. R., KEAR, B. H. and OBLAK, J. M., *Met. Trans.* **4** (1973) 355.

[11] THOMPSON, N., *Proc. Phys. Soc.* **66B** (1953) 481.

[12] WEERTMAN, J., *Phil. Mag.* **8** (1963) 967.

[13] MARCINKOWSKI, M. J., BROWN, N. and FISHER, R. M., *Acta Met.* **9** (1961) 129.

[14] KEAR, B. H., Proc. Int. Conf. on the Strength of Metals and Alloys, Tokyo (1967) 669.

[15] MIKKOLA, D. E. and COHEN, J. B., *Acta Met.* **14** (1966) 105.

[16] KEAR, B. H., GIAMEI, A. F. and OBLAK, J. M., *Scripta Met.* **4** (1970) 567 ; **3** (1969) 123.

[17] GRINBERG, B. A., *Fiz. Metal. Metalloved* **15** (1963) 486.

[18] FLINN, P. A., *Trans. Met. Soc. AIME* **218** (1960) 145.

[19] KEAR, B. H. and WILSDORF, H. G. F., *Trans. Met. Soc. AIME* **224** (1962) 382.

[20] GIAMEI, A. F., OBLAK, J. M., KEAR, B. H. and RAND, W. H., Proc. 29th Annual Meeting EMSA (1971) 112.

[21] KEAR, B. H. and HORNBECKER, M. F., *Trans. ASM* **59** (1966) 155.

[22] ENAMI, K. and NENNO, S., *J. Phys. Soc. Japan* **25** (1968) 1517.

[23] CORNWELL, L. R., PURDY, G. R. and EMBURY, J. D., *Phys. Stat. Sol.* **35** (1969) K1.

[24] OBLAK, J. M. and RAND, W. H., Proc. 32nd Annual Meeting EMSA (1974).

[25] THORNTON, P. H., DAVIES, R. G. and JOHNSTON, T. L., *Met. Trans.* **1** (1970) 207.

[26] LEVERANT, G. R., GELL, M. and HOPKINS, S. W., *Mats. Sci. & Eng.* **8** (1971) 123.

[27] KEAR, B. H., COPLEY, S. M. and PIEARCEY, B. J., *Proc. Sixth Int. Congress Electron Microscopy, Japan* **1** (1966) 397.

[28] DELEHOUZEE, L. and DERUYTTERE, A., *Acta Met.* **15** (1967) 727.

[29] BEESTON, B. E. P., DILLAMORE, I. L. and SMALLMAN, R. E., *Metal. Sci. J.* **2** (1968) 12.

[30] BEESTON, B. E. P. and FRANCE, L. K., *J. Inst. Metals* **96** (1968) 105.

[31] HIRTH, J. P., *J. Appl. Phys.* **32** (1961) 700.

[32] GALLAGHER, P. C. J., *Phys. Stat. Sol.* **16** (1966) 95.

[33] KEAR, B. H., GIAMEI, A. F., LEVERANT, G. R. and OBLAK, J. M., *Scripta Met.* **3** (1969) 455.

[34] KEAR, B. H., LEVERANT, G. R. and OBLAK, J. M., *Trans. ASM* **62** (1969) 639.

[35] GUIMIER, A. and STRUDEL, J. L., Second Intl. Conf. on the Strength of Metals and Alloys, *ASM* **3** (1970) 1145.

[36] KHOBAIB, M., STRUTT, P. R. and KEAR, B. H., Proc. 32nd Annual Meeting EMSA (1974).

[37] KEAR, B. H., OBLAK, J. M. and GIAMEI, A. F., Second Int. Conf. on the Strength of Metals and Alloys, *ASM* **3** (1970) 1155.

[38] KEAR, B. H. and PIEARCEY, B. J., *Trans. AIME* **239** (1967) 1209.